

Smoothing and mean-covariance estimation of functional data with a Bayesian hierarchical model

Jingjing Yang ^{*}, Hongxiao Zhu [†], Dennis D. Cox ^{*}

Abstract.

Functional data, with basic data units being functions (e.g., curves, surfaces) varying over continuums, are frequently encountered nowadays. While many statistical inference tools have been developed, the issue of smoothing all functional observations simultaneously is less studied. Most available methods either treat functional data as fully observed while ignoring measurement error, or perform smoothing to each individual curve in a separate preprocessing step. The latter approach, not only fails to borrow strength across curves, but also may introduce the risk of removing important systematic patterns that are common across all curves. In this paper, we propose a unified Bayesian framework to perform simultaneous smoothing as well as mean-covariance estimation. This novel approach borrows strength across all curves through assuming that functional observations are independent Gaussian processes subject to measurement error. The amount of smoothness is controlled by the common prior parameters. In addition to smoothing, the proposed approach also provides nonparametric estimation of the mean curve and the covariance surface through assuming a Gaussian process prior for the mean and an Inverse-Wishart process prior for the covariance. The proposed Bayesian framework is general enough to accommodate functional observations either on common or uncommon grids, and allows both stationary and non-stationary covariance structures. Simulation and real data analysis demonstrate that the proposed approach achieves better smoothing accuracy than existing methods and comparable mean-covariance estimation results; it can also retain systematic patterns that are common across all functional observations. Although the mean-covariance estimation from a Bayesian regression model is by no means a new topic, this novel framework provides a Bayesian counterpart that gives comparable estimation results to existing approaches.

Keywords: functional data, smoothing, Bayesian hierarchical model, Gaussian process, Matérn covariance function, empirical Bayes

1 Introduction

As more and more digital data are being collected in modern experiments and daily lives, great efforts have been made to store, process, and analyze data in “functional” form — data that are realizations of random functions varying over a continuum such as time, spatial location or wavelength (Ramsay and Silverman 2002). Since Ramsay and

^{*}Department of Statistics, Rice University, Houston, TX, USA, yjingj@gmail.com, dcox@rice.edu

[†]Department of Statistics, Virginia Tech, Blacksburg, VA 24061, hongxiao@vt.edu

Dalzell (1991) first coined the term “functional data analysis (FDA)”, numerous papers have been published on inferential methodologies, which makes FDA a dynamic research area in statistics. One salient feature of functional data is that, although the functions are inherently smooth and infinite dimensional, they can only be collected discretely with measurement error. Therefore smoothing is often the first and an inevitable step in FDA. Through smoothing one aims to recover the smooth functions from discretized measurements and reduce the effect of noise. More accurately recovered functions lead to less biased results in further analyses. For example, Hitchcock et al. (2006) showed that working with smoothed functional data gave more accurate classification than naively treating the raw data as vectors and applying multivariate methods.

Despite the importance of smoothing, many existing statistical methods treat functional data as fully observed while ignoring the measurement error (Hall et al. 2001; Cardot et al. 2003; Zhu and Cox 2009; Zhu et al. 2010). Although it is fine to do so when the influence of measurement error is negligible, pre-smoothing is often necessary if the level of measure error is relatively high. Ramsay (2006) reviewed several nonparametric smoothing methods including basis expansion, kernel smoothing and smoothing splines. In these methods smoothing is performed on each individual curve independently, and separately from the following statistical inference. As a result, such methods often fail to borrow strength across all observations. For example, the amount of smoothness can vary across the curves, and smoothing will become difficult or even intractable when data are sparsely observed. Another potential drawback of these methods is the blurring/wiping-out of systematic effects.

A real spectroscopy data example from Section 5.1 is shown in Figure 1 as a motivation of a simultaneously smoothing method, which demonstrates that the wiggles in the raw data (Figure 1(a)) are completely wiped out after kernel smoothing is performed to each curve (Figure 1(b)). Even though the splines smoothing method (Figure 1(c)) kept local features for each curve, there exists less consistent smoothness among all curves due to smoothing individually. For example, in the area around $t=600$, the small wiggles were smoothed out for some of the curves (e.g., red, green) but kept for the others (e.g., blue). Here, the smoothing estimates from the novel Bayesian method (described in Section 2) in Figure 1(d) were shown as an example of simultaneously smoothing which borrows strength across all data. Although in this particular case the wiggles may be caused by systematic patterns, we believe that such repeated features could carry important information therefore one may wish to retain those local features in the smoothing stage.

In this paper, we propose a unified Bayesian hierarchical model (BHM) to smooth all functional observations simultaneously and provide a nonparametric mean-covariance estimation. The proposed approach borrows strength across all functions through assuming an error-prone Gaussian process likelihood, a Gaussian process prior for the mean curves and an inverse-Wishart process prior for the covariance surface. The hyper-parameters are determined from the data using heuristic empirical Bayes methods. Posterior inference is performed through Markov chain Monte Carlo (MCMC) algorithms. This novel Bayesian framework is flexible to accommodate functional observations on common or uncommon grids, as well as moderately sparse observations;

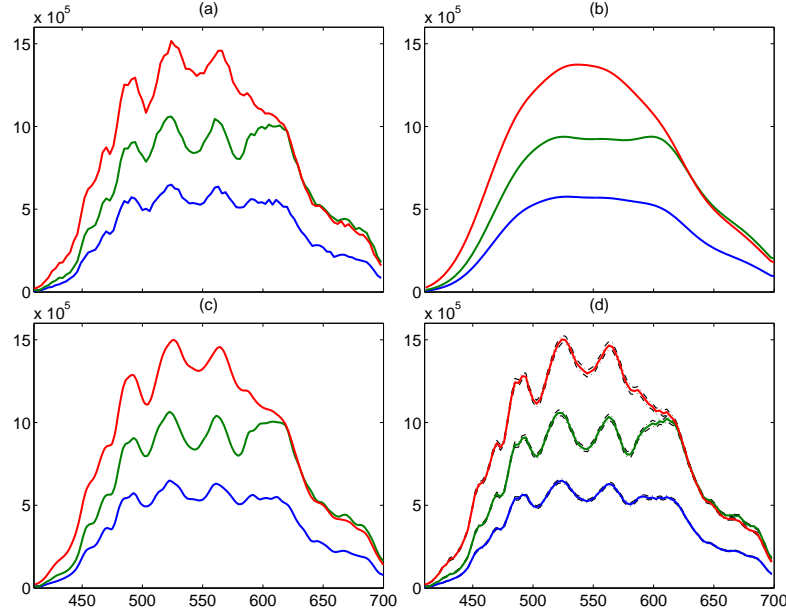


Figure 1: Three example raw spectroscopy curves were plotted in (a), with corresponding smoothed estimates from Kernel smoothing method in (b), Splines smoothing method in (c), and Bayesian smoothing method along with 95% point wise credible intervals (black dashed curve) in (d).

it is also appropriate for functional data with both stationary and non-stationary covariance structures. We demonstrate the performance of the proposed method using both simulation studies and real case studies of spectroscopy/metabolic data. As compared with other individually nonparametric smoothing methods (e.g., smoothing splines, kernel smoothing), the proposed approach can recover the true signals more accurately and is able to retain systematic patterns common across curves. Regarding the mean-covariance estimation, the proposed approach provides better results than the sample estimates, and comparable/better results than the principal analysis by conditional expectation (PACE) of Yao et al. (2005).

The rest of this article is organized as follows. We outline the details of the proposed Bayesian hierarchical model in Section 2 as well as the heuristic empirical Bayes approach used to determine hyper-priors. We describe the MCMC algorithm for posterior inference in Section 3. Results on simulation and real case studies are presented in Sections 4 and 5, respectively. A discussion is provided in Section 6.

2 A unified Bayesian hierarchical model for smoothing and estimation

2.1 Bayesian hierarchical framework

Suppose that the functional data contain n independent trajectories, denoted by $\{Y_i(\cdot); i = 1, 2, \dots, n\}$, and the i^{th} trajectory has p_i measurements on the grid $\mathbf{t}_i = \{t_{i1}, \dots, t_{ip_i}\}$. Further assume that the i^{th} trajectory $Y_i(\cdot)$ depends on an underlying Gaussian process $Z_i(t), t \in \mathcal{T}$ through the following model:

$$Y_i(t_{ij}) = Z_i(t_{ij}) + \epsilon_{ij}; \quad t_{ij} \in \mathcal{T}, \quad i = 1, \dots, n, \quad j = 1, \dots, p_i, \quad (1)$$

where $\{Z_i(\cdot)\}$ are independent and identically distributed (i.i.d.) Gaussian processes with mean function $\mu(\cdot)$ and covariance kernel $\Sigma(\cdot, \cdot)$, denoted by $Z_i \sim GP(\mu, \Sigma)$. The covariance kernel satisfies that $\Sigma(s, t) = E[(Z_i(s) - \mu(s))(Z_i(t) - \mu(t))]$. The error term $\{\epsilon_{ij}\}$ are assumed to be i.i.d. normal, i.e., $\epsilon_{ij} \sim N(0, \sigma_\epsilon^2)$ and independent of $Z_i(\cdot)$. We assume the following priors for the model parameters $\sigma_\epsilon^2, \mu(\cdot)$, and $\Sigma(\cdot, \cdot)$:

$$\sigma_\epsilon^2 \sim \text{Inv-Gamma}(a_\epsilon, b_\epsilon), \quad (\mu \mid \Sigma) \sim GP\left(\mu_0, \frac{1}{c}\Sigma\right), \quad \Sigma \sim \text{IWP}(\delta, \Psi), \quad (2)$$

where $\text{Inv-Gamma}(a_\epsilon, b_\epsilon)$ denotes an Inverse-Gamma distribution with shape parameter a_ϵ and scale parameter b_ϵ , and $c > 0$ is a constant. Here $\text{IWP}(\delta, \Psi)$ denotes the Inverse-Wishart process (IWP), which is defined such that on any finite grid $\mathbf{t} = \{t_1, t_2, \dots, t_p\}$, the projection $\Sigma(\mathbf{t}, \mathbf{t})$ is Inverse-Wishart distributed, i.e., $\Sigma(\mathbf{t}, \mathbf{t}) \sim \text{IW}(\delta, \Psi(\mathbf{t}, \mathbf{t}))$. Notice that the Inverse-Wishart distribution used here follows the parametrization of Dawid (1981). In particular, a symmetric and positive definite matrix $\Sigma(\mathbf{t}, \mathbf{t})$ is said to be $\text{IW}(\delta, \Psi(\mathbf{t}, \mathbf{t}))$ distributed if $\mathbf{K} = \Sigma(\mathbf{t}, \mathbf{t})^{-1}$ is Wishart distributed with degrees of freedom $\delta + p - 1$ and scale matrix $\Psi(\mathbf{t}, \mathbf{t})^{-1}$, i.e., $\mathbf{K} \sim W(\delta + p - 1, \Psi(\mathbf{t}, \mathbf{t})^{-1})$.

The advantages of adopting Dawid (1981)'s parameterization for Inverse-Wishart distribution is two-fold: the parameter δ does not vary with the dimension of \mathbf{t} , and the resulting distribution is consistent under marginalization. These properties facilitate the well-definedness of the IWP prior for $\Sigma(\cdot, \cdot)$ when the number of grid points p approaches infinity. This result is summarized in Proposition 2.1, and the the proof can be done following the proof of Lemma 2 in the Appendix of Zhu et al. (2011).

Proposition 2.1 *Let $\mathcal{T} \subseteq \mathbb{R}$ be a compact set and $\delta > 4$ be a positive integer. Suppose that $\Psi : \mathcal{T} \times \mathcal{T} \rightarrow \mathbb{R}$ is a symmetric and positive definite mapping, i.e., any evaluation of Ψ on a finite grid $\mathbf{t} \times \mathbf{t} \subseteq \mathcal{T} \times \mathcal{T}$ gives a symmetric and positive definite matrix. Then there exists a unique probability measure λ on $(\mathbb{R}^{\mathcal{T} \times \mathcal{T}}, \mathcal{B}(\mathbb{R}^{\mathcal{T} \times \mathcal{T}}))$ such that for any finite discretization \mathbf{t} , $\lambda_{\mathbf{t} \times \mathbf{t}} = \text{IW}(\delta, \Psi(\mathbf{t}, \mathbf{t}))$. We denote $\lambda = \text{IWP}(\delta, \Psi)$.*

In the prior $\Sigma \sim \text{IWP}(\delta, \Psi)$, smaller value of δ corresponds to less informative prior. The parameter Ψ controls the a priori covariance structure. To encourage a smoother

estimation to the covariance, we set $\Psi(\cdot, \cdot) = \sigma_s^2 A(\cdot, \cdot)$, where σ_s^2 is the marginal variance and $A(\cdot, \cdot)$ is a smooth correlation kernel which can take either stationary or non-stationary forms. The structure of $A(\cdot, \cdot)$ may be determined by one or more hyper parameters. In this paper, we use the Matérn correlation structure as an example, which leads to

$$\Psi(t_i, t_j) = \sigma_s^2 \text{Matern}_{cor}(|t_i - t_j|; \text{length.scale } \rho, \text{ order } \nu),$$

where the Matérn correlation function is defined as

$$\text{Matern}_{cor}(d; \rho, \nu) = \frac{1}{\Gamma(\nu)2^{\nu-1}} \left(\sqrt{2\nu} \frac{d}{\rho} \right)^\nu K_\nu \left(\sqrt{2\nu} \frac{d}{\rho} \right), \quad \rho > 0, \nu > 0.$$

Here $K_\nu(\cdot)$ is the modified Bessel function of the second kind. Both ν and ρ can influence the smoothness of the signal estimates $Z_i(\cdot)$. The Matérn function has many nice properties which are given in Stein (1999), e.g., ensuring symmetry and positive definite as a covariance kernel. We choose $\nu > 2$ so that the signals from a Gaussian process with this covariance will be $\lfloor \nu - 1 \rfloor$ times differentiable. It is also convenient to take ν to be an integer plus 1/2, in which case the Matérn correlation function will have a closed-form expression. In particular, if $\nu = 2.5$, the correlation function $A(\cdot, \cdot)$ takes the form

$$A(t_i, t_j) = \left(1 + \frac{\sqrt{5}|t_i - t_j|}{\rho} + \frac{5(|t_i - t_j|)^2}{3\rho^2} \right) \exp \left(-\frac{\sqrt{5}|t_i - t_j|}{\rho} \right). \quad (3)$$

Note that the Matérn structure is sensitive to the smoothing parameters ρ and ν , which usually leads to unstable estimation of the Matérn structure. Indeed, Zhang (2004) has pointed out in a geostatistic setup that not all three parameters (σ_s^2, ρ, ν) in the Matérn class can be estimated consistently if data are observed in an increasing density in a fixed domain. To ensure a stable covariance estimation, we take fixed values for ν and ρ based on empirically estimated correlation structure. The hyper-prior for σ_s^2 is set to be $\sigma_s^2 \sim G(a_s, b_s)$, i.e., a Gamma distribution with shape parameter a_s and inverse scale parameter b_s .

Although the above Bayesian hierarchical framework is constructed in infinite dimensional function space, posterior calculation can only be conducted in a finite manner. Since we assume latent Gaussian processes $\{Z_i(\cdot)\}$ in our model, posterior inference will be performed similarly as that in Bayesian Gaussian process regression. In particular, the latent processes $\{Z_i(\cdot)\}$ and the parameters $\mu(\cdot)$, $\Sigma(\cdot, \cdot)$ will be inferred on a finite grid, and the inference on non-grid points, if needed, can be obtained by posterior prediction. Guided by this intuition, we will represent the likelihood corresponding to model (1) and the prior in (2) in multivariate forms through evaluating the functions on a finite grid. Denote $Y(\mathbf{t}_i)$ by $\mathbf{Y}_{\mathbf{t}_i}$ and $Z_i(\mathbf{t}_i)$ by $\mathbf{Z}_{\mathbf{t}_i}$, model (1) implies that

$$\mathbf{Y}_{\mathbf{t}_i} | \mathbf{Z}_{\mathbf{t}_i}, \sigma_\epsilon^2 \sim N(\mathbf{Z}_{\mathbf{t}_i}, \sigma_\epsilon^2 \mathbf{I}), \quad i = 1, \dots, n, \quad (4)$$

$$\mathbf{Z}_{\mathbf{t}_i} | \mu(\mathbf{t}_i), \Sigma(\mathbf{t}_i, \mathbf{t}_i) \sim N(\mu(\mathbf{t}_i), \Sigma(\mathbf{t}_i, \mathbf{t}_i)), \quad (5)$$

where \mathbf{I} is a $p_i \times p_i$ identity matrix. Since the grids $\{\mathbf{t}_i; i = 1, 2, \dots, n\}$ are not required to be common across i , we evaluate the GP and IWP prior distributions in (2) on the

pooled grid $\mathbf{t} = \cup_{i=1}^n \mathbf{t}_i$ and assume that \mathbf{t} is a vector of length p . Denote $\mu(\mathbf{t})$ by $\boldsymbol{\mu}$, $\mu_0(\mathbf{t})$ by $\boldsymbol{\mu}_0$, $\Sigma(\mathbf{t}, \mathbf{t})$ by $\boldsymbol{\Sigma}$ and $\Psi(\mathbf{t}, \mathbf{t})$ by $\boldsymbol{\Psi}$, then

$$\boldsymbol{\mu} \mid \boldsymbol{\Sigma} \sim N\left(\boldsymbol{\mu}_0, \frac{1}{c}\boldsymbol{\Sigma}\right), \quad \boldsymbol{\Sigma} \sim \text{IW}(\delta, \boldsymbol{\Psi}). \quad (6)$$

The multivariate representations in (4)–(6) enable us to write the joint posterior distribution of $(\{Z_i(\mathbf{t})\}, \boldsymbol{\mu}, \boldsymbol{\Sigma}, \sigma_\epsilon^2, \sigma_s^2)$, based on which posterior sampling can be performed using MCMC algorithms; details are presented in Section 3. The posterior means of $\{Z_i(\mathbf{t})\}$ will be treated as the smoothed signals.

2.2 Prior parameter setup

The proposed Bayesian hierarchical framework described in Section 2.1 involves several hyper-parameters: $(c, \boldsymbol{\mu}_0, \nu, \rho, a_\epsilon, b_\epsilon, a_s, b_s)$. Their values are determined using empirical methods. In particular, we take $c = n$, which corresponds to scale the prior covariance of the mean curve by the reciprocal of the number of observations n . The value of $\boldsymbol{\mu}_0$ can be taken as the smoothed sample mean of $\{\mathbf{Y}_{\mathbf{t}_i}\}$. To facilitate stable covariance estimation and encourage smooth covariance structure, we take ν and ρ as their empirical estimates respectively. For example, empirical estimates $\hat{\nu}$ and $\hat{\rho}$ can be obtained by minimizing the mean square error between an empirical correlation estimate and $\text{Matern}_{\text{cor}}(\mathbf{D}; \rho, \nu)$ with distance matrix \mathbf{D} , such that $\rho > 0$, $\nu \geq 2.5$.

The values for $(a_\epsilon, b_\epsilon, a_s, b_s)$ are decided by a heuristic empirical Bayes approach, described as follows. First, we find empirical estimates for $\{\sigma_\epsilon^2, \sigma_s^2\}$ from (7) and (8):

- The value of $\hat{\sigma}_\epsilon^2$ can be easily obtained by a differencing technique (Von Neumann 1941)

$$\hat{\sigma}_\epsilon^2 = \frac{1}{2 \sum_{i=1}^n (p_i - 1)} \sum_{i=1}^n \sum_{j=1}^{p_i-1} (Y_i(t_{i(j+1)}) - Y_i(t_{ij}))^2. \quad (7)$$

- A moment estimator of σ_s^2 can be derived by taking expectation (with respect to the prior distribution of $\boldsymbol{\Sigma}$) and applying a trace operator to both sides of $\text{Cov}(Y(\mathbf{t})) = \boldsymbol{\Sigma} + \sigma_\epsilon^2 \mathbf{I}$, which gives

$$\begin{aligned} \text{trace}(E\{\text{Cov}(Y(\mathbf{t}))\}) &= \frac{\text{trace}(\boldsymbol{\Psi})}{\delta - 2} + \sigma_\epsilon^2 \text{trace}(\mathbf{I}) = \frac{\sigma_s^2 p}{\delta - 2} + p\sigma_\epsilon^2, \\ \hat{\sigma}_s^2 &\approx \frac{\text{trace}(E\{\text{Cov}(Y(\mathbf{t}))\}) - p\hat{\sigma}_\epsilon^2}{p/(\delta - 2)}, \end{aligned} \quad (8)$$

where p is the length of the pooled grid \mathbf{t} , $\hat{\sigma}_\epsilon^2$ is given by (7), and $E\{\text{Cov}(Y(\mathbf{t}))\}$ is estimated by an empirical method, e.g., the smoothed sample covariance estimate used in Yao et al. (2005).

Next, we set values for $(a_\epsilon, b_\epsilon, a_s, b_s)$ such that $E(1/\sigma_\epsilon^2) = a_\epsilon/b_\epsilon = 1/\hat{\sigma}_\epsilon^2$, $\text{Var}(1/\sigma_\epsilon^2) = a_\epsilon/b_\epsilon^2 = w_\epsilon/\hat{\sigma}_\epsilon^2$, $E(\sigma_s^2) = a_s/b_s = \hat{\sigma}_s^2$, $\text{Var}(\sigma_s^2) = a_s/b_s^2 = w_s\hat{\sigma}_s^2$, where w_ϵ, w_s are

appropriately chosen constants that are used to adjust for the respective prior variances. Note that in this model, there does exist unidentifiable issue for the magnitude parameter σ_s^2 in the IWP prior. Therefore, the average diagonal value of the empirical covariance estimate can be used as a guide to choose a proper value for w_s .

3 Posterior inference using Markov chain Monte Carlo

To develop the joint posterior distribution, we denote the observed data by $\mathbf{Y} = \{\mathbf{Y}_{\mathbf{t}_1}, \mathbf{Y}_{\mathbf{t}_2}, \dots, \mathbf{Y}_{\mathbf{t}_n}\}$, and denote the underlying Gaussian processes evaluated on the observational grids by $\mathbf{Z} = \{\mathbf{Z}_{\mathbf{t}_1}, \mathbf{Z}_{\mathbf{t}_2}, \dots, \mathbf{Z}_{\mathbf{t}_n}\}$, on the pooled grid by $\tilde{\mathbf{Z}} = \{Z_1(\mathbf{t}), Z_2(\mathbf{t}), \dots, Z_n(\mathbf{t})\}$. Since $\mathbf{t} = \cup_i \mathbf{t}_i$, we denote $\mathbf{Z}^* = \tilde{\mathbf{Z}} \setminus \mathbf{Z}$. Then $\mathbf{Z}^* = \{\mathbf{Z}_{\mathbf{t}_1^*}, \mathbf{Z}_{\mathbf{t}_2^*}, \dots, \mathbf{Z}_{\mathbf{t}_n^*}\}$, $\mathbf{Z}_{\mathbf{t}_i^*} = Z_i(\mathbf{t}_i^*)$ and $\mathbf{t}_i^* = \mathbf{t} \setminus \mathbf{t}_i$. The joint posterior density of all parameters can be written as

$$\begin{aligned} f(\tilde{\mathbf{Z}}, \boldsymbol{\mu}, \boldsymbol{\Sigma}, \sigma_\epsilon^2, \sigma_s^2 | \mathbf{Y}) &\propto f(\mathbf{Y} | \tilde{\mathbf{Z}}, \sigma_\epsilon^2) f(\tilde{\mathbf{Z}} | \boldsymbol{\mu}, \boldsymbol{\Sigma}) f(\sigma_\epsilon^2) f(\boldsymbol{\mu} | \boldsymbol{\Sigma}) f(\boldsymbol{\Sigma} | \sigma_s^2) f(\sigma_s^2) \\ &\propto f(\mathbf{Y} | \mathbf{Z}, \sigma_\epsilon^2) f(\mathbf{Z}^* | \mathbf{Z}, \boldsymbol{\mu}, \boldsymbol{\Sigma}) f(\mathbf{Z} | \boldsymbol{\mu}, \boldsymbol{\Sigma}) f(\sigma_\epsilon^2) f(\boldsymbol{\mu} | \boldsymbol{\Sigma}) f(\boldsymbol{\Sigma} | \sigma_s^2) f(\sigma_s^2). \end{aligned} \quad (9)$$

Here we have factored the joint prior of $\tilde{\mathbf{Z}}$ as $f(\tilde{\mathbf{Z}} | \boldsymbol{\mu}, \boldsymbol{\Sigma}) = f(\mathbf{Z}^* | \mathbf{Z}, \boldsymbol{\mu}, \boldsymbol{\Sigma}) f(\mathbf{Z} | \boldsymbol{\mu}, \boldsymbol{\Sigma})$, which enables us to update \mathbf{Z} and \mathbf{Z}^* alternatively using a Gibbs sampler. To design a MCMC algorithm using the Gibbs sampler, we need to derive conditional distributions of all parameters, including the smoothed signals \mathbf{Z} and \mathbf{Z}^* , and the model parameters $\boldsymbol{\mu}, \boldsymbol{\Sigma}, \sigma_s^2, \sigma_\epsilon^2$. For brevity, we only present the conditional posterior distributions of \mathbf{Z} and \mathbf{Z}^* in Section 3.1. The conditional posteriors for the rest of the parameters are easy to derive due to the conjugacy of the priors.

3.1 Conditional posterior for the smoothed signals

In case that all functional data are observed on a common grid, i.e., $\mathbf{t}_i \equiv \mathbf{t}$ for $i = 1, 2, \dots, n$, \mathbf{Z}^* vanishes, and the conditional posterior distribution of $\mathbf{Z}_{\mathbf{t}_i}$ can be derived from $f(\mathbf{Z}_{\mathbf{t}_i} | \mathbf{Y}_{\mathbf{t}_i}, \boldsymbol{\mu}, \boldsymbol{\Sigma}) \propto f(\mathbf{Y}_{\mathbf{t}_i} | \mathbf{Z}_{\mathbf{t}_i}, \boldsymbol{\mu}, \boldsymbol{\Sigma}) f(\mathbf{Z}_{\mathbf{t}_i} | \boldsymbol{\mu}, \boldsymbol{\Sigma})$, which gives

$$\begin{aligned} (\mathbf{Z}_{\mathbf{t}_i} | \mathbf{Y}_{\mathbf{t}_i}, \boldsymbol{\mu}, \boldsymbol{\Sigma}) &\sim N(\tilde{\boldsymbol{\mu}}_i, \tilde{\mathbf{V}}_i), \\ \tilde{\mathbf{V}}_i &= ((1/\sigma_\epsilon^2)\mathbf{I} + \boldsymbol{\Sigma}^{-1})^{-1}, \\ \tilde{\boldsymbol{\mu}}_i &= \tilde{\mathbf{V}}_i((1/\sigma_\epsilon^2)\mathbf{Y}_{\mathbf{t}_i} + \boldsymbol{\Sigma}^{-1}\boldsymbol{\mu}(\mathbf{t})). \end{aligned} \quad (10)$$

In case that functional data are collected on uncommon grids, we will update $\mathbf{Z}_{\mathbf{t}_i}$ from (10) with $\boldsymbol{\Sigma} = \boldsymbol{\Sigma}(\mathbf{t}_i, \mathbf{t}_i)$, $\mathbf{t} = \mathbf{t}_i$. Then update $\mathbf{Z}_{\mathbf{t}_i^*}$ from

$$\begin{aligned} (\mathbf{Z}_{\mathbf{t}_i^*} | \mathbf{Z}_{\mathbf{t}_i}, \boldsymbol{\mu}, \boldsymbol{\Sigma}) &\sim N(\boldsymbol{\mu}_i^*, \mathbf{V}_i^*), \\ \boldsymbol{\mu}_i^* &= \boldsymbol{\mu}(\mathbf{t}_i^*) + \boldsymbol{\Sigma}(\mathbf{t}_i^*, \mathbf{t}_i) \boldsymbol{\Sigma}(\mathbf{t}_i, \mathbf{t}_i)^{-1} (\mathbf{Z}_{\mathbf{t}_i} - \boldsymbol{\mu}(\mathbf{t}_i)), \\ \mathbf{V}_i^* &= \boldsymbol{\Sigma}(\mathbf{t}_i^*, \mathbf{t}_i^*) - \boldsymbol{\Sigma}(\mathbf{t}_i^*, \mathbf{t}_i) \boldsymbol{\Sigma}(\mathbf{t}_i, \mathbf{t}_i)^{-1} \boldsymbol{\Sigma}(\mathbf{t}_i, \mathbf{t}_i^*). \end{aligned} \quad (11)$$

3.2 MCMC algorithm

Based on conditional posterior distributions derived from (9), we design a MCMC algorithm for posterior sampling. Details of the steps are listed as follows:

Step 0: Set initial values of $(\mathbf{Z}, \boldsymbol{\mu}, \sigma_\epsilon^2)$ to be empirical estimates from the data where \mathbf{Z} can be estimated by the raw data \mathbf{Y} ; let the initial value of $\boldsymbol{\Sigma}$ be an identity matrix; and set prior parameters $(c, \boldsymbol{\mu}_0, \nu, \rho, a_\epsilon, b_\epsilon, a_s, b_s)$ as described in Section 2.2.

Step 1: Conditional on \mathbf{Y} and current values of $(\boldsymbol{\mu}, \boldsymbol{\Sigma})$, update \mathbf{Z} and \mathbf{Z}^* . In the general case that all data are observed on uncommon grids, update \mathbf{Z} and \mathbf{Z}^* from (10) and (11) alternatively. In case of common grids, update \mathbf{Z} from (10).

Step 2: Conditional on \mathbf{Y} and current value of \mathbf{Z} , update the noise variance σ_ϵ^2 by

$$(\sigma_\epsilon^2 | \mathbf{Y}, \mathbf{Z}) \sim \text{Inv-Gamma} \left(a_\epsilon + \frac{\sum_{i=1}^n p_i}{2}, \quad b_\epsilon + \frac{1}{2} \sum_{i=1}^n [(\mathbf{Y}_{t_i} - \mathbf{Z}_{t_i})^T (\mathbf{Y}_{t_i} - \mathbf{Z}_{t_i})] \right).$$

Step 3: Conditioning on current values of $\tilde{\mathbf{Z}} = \mathbf{Z} \cup \mathbf{Z}^*$ and $\boldsymbol{\Sigma}$, update $\boldsymbol{\mu}$ from

$$(\boldsymbol{\mu} | \tilde{\mathbf{Z}}, \boldsymbol{\Sigma}) \sim N \left(\frac{1}{n+c} \left(\sum_{i=1}^n \mathbf{Z}_i(t) + c\boldsymbol{\mu}_0 \right), \quad \frac{1}{n+c} \boldsymbol{\Sigma} \right).$$

Step 4: Conditional on current values of $\tilde{\mathbf{Z}} = \mathbf{Z} \cup \mathbf{Z}^*$ and $\boldsymbol{\mu}$, update $\boldsymbol{\Sigma}$ from

$$(\boldsymbol{\Sigma} | \tilde{\mathbf{Z}}, \boldsymbol{\mu}) \sim IW(n + \delta + 1, \mathbf{Q}), \quad \mathbf{Q} = (\tilde{\mathbf{Z}} - \boldsymbol{\mu}\mathbf{J})(\tilde{\mathbf{Z}} - \boldsymbol{\mu}\mathbf{J})^T + c(\boldsymbol{\mu} - \boldsymbol{\mu}_0)(\boldsymbol{\mu} - \boldsymbol{\mu}_0)^T + \sigma_s^2 \mathbf{A},$$

where $\tilde{\mathbf{Z}}$ denote a matrix with the i th column $\mathbf{Z}_i(t)$, $\mathbf{J} = (1, \dots, 1)$ has length p , and matrix \mathbf{A} has elements given by equation (3).

Step 5: Given current value of $\boldsymbol{\Sigma}$, update σ_s^2 from

$$(\sigma_s^2 | \boldsymbol{\Sigma}) \sim \text{Gamma} \left(a_s + \frac{(\delta + p - 1)p}{2}, \quad b_s + \frac{1}{2} \text{trace}(\mathbf{A}\boldsymbol{\Sigma}^{-1}) \right).$$

Repeat Step 1-5 for a large number of iterations until convergence.

When one implementing this MCMC algorithm, it is possible to encounter computation issues regarding taking inverse of a matrix that is nearly singular, sampling random multivariate normal samples with a covariance matrix that is not positive definite, and sampling random inverse wishart samples with a scale matrix that is not positive definite or nearly singular. In our case studies, we took strategies such as general inverse and converting a non-positive definite matrix to a positive definite by replacing its non-positive eigenvalues by a fairly small positive number.

In all case studies in Section 4 and Section 5, we have collected 10,000 MCMC iterations after a burn-in period of 2,000 iterations. The convergence of the chain has been diagnosed using empirical convergence test, e.g., the Gelman and Rubin diagnostic method (Gelman and Rubin 1992; Särkkä and Aki 2014).

4 Simulation studies

Two simulation studies are performed for functional data with both stationary and non-stationary covariances and for the cases of both common and uncommon grids.

4.1 Simulation 1: functional data with stationary covariance

Functional data with stationary covariance were generated on both common and uncommon grids. The underlying smooth functions were generated from a Gaussian process with mean $\mu(t) = 3\sin(4t)$, $t \in [0, \pi/2]$ and covariance kernel $\Sigma(s, t) = 5\text{Matern}_{cor}(|s - t|; \rho = 1/2, \nu = 3.5)$. Each data set contains $n = 50$ observations. The common grid contains $p = 80$ equally spaced grid points on $[0, \pi/2]$. Noise terms $\{\epsilon_{ij}; i = 1, \dots, n, j = 1, \dots, p\}$ were simulated from i.i.d. $N(0, \sigma_\epsilon = \sqrt{5}/2)$ and were added to the smooth functions, resulting in signal to noise ratio (SNR) around 2 for the final data. In the uncommon grid case, we take the data from the common grid case and randomly select function values on 60% of the grid points, which results in moderately sparse functional data (also a uncommon-grid case). Two example curves for the common grid and uncommon grid cases were plotted Figure 2 in (a) and (b) respectively; see the grey lines/line segments.

Based on the data generated above, we apply the MCMC algorithm described in Section 3.2 with $\delta = 30$ to obtain the posterior samples. Take the common grid case as an example, initial empirical estimation gives $\hat{\rho} = 0.523$, $\hat{\nu} = 2.503$, $\hat{\sigma}_\epsilon^2 = 1.239$ and $\hat{\sigma}_s^2 = 100.333$. Setting $\{w_\epsilon = 1, w_s = 1\}$, we get the prior parameters $\{a_\epsilon = 0.807, b_\epsilon = 1, a_s = 100.333, b_s = 1\}$. The posterior mean of the parameters were calculated by averaging 10,000 posterior samples. The posterior mean for σ_ϵ^2 is 1.236 with 95% credible interval $[1.181, 1.295]$ and for σ_s^2 is 110.4 with 95% credible interval $[93.793, 126.435]$. In Figure 2 (a) and (b), we display the smoothed curves (black solid lines) together with the raw data (grey lines/line segments), 95% point wise credible interval (black dashed lines), and the true data (blue dots) for the common and uncommon grid cases, respectively. The heat maps of the posterior mean for the correlation are shown in (c)/(d) for cases with common/uncommon grids. We also presented the heat map of the sample correlation estimate (for the common grid case) in (e), and the true underlying correlation heat map in (f). These plots show that our method can recover the smoothed signals well for both common grid and uncommon grid cases; it also provides smoother correlation estimate (than the sample estimate). Furthermore, the smoothing and the mean-covariance estimation results in the uncommon grid case are almost as good as the common grid case even though around 40% of the grid points are missing in each trajectory.

To further compare the performance of the proposed method with alternative ones. We consider three alternative smoothing methods – the *best possible least square* (BLS) estimate, the nonparametric cubic splines applied to each individual curve (Spline), and the kernel smoothing with local polynomials applied to each individual curve (Kernel). The BLS method serves as an “oracle” model, in which the smoothed curves are estimated by the conditional mean of the latent Gaussian processes, while assuming

that the true mean and covariance of the latent processes are known. In the common grid case, the conditional mean and covariance for each signal can be written by

$$\begin{aligned} E\{\mathbf{Z}_i|\mathbf{Y}_i, \boldsymbol{\mu}, \boldsymbol{\Sigma}\} &= \boldsymbol{\mu} + \boldsymbol{\Sigma}(\boldsymbol{\Sigma} + \sigma_\epsilon^2 \mathbf{I})^{-1}(\mathbf{Y}_i - \boldsymbol{\mu}), \\ \text{Cov}(\mathbf{Z}_i|\mathbf{Y}_i, \boldsymbol{\mu}, \boldsymbol{\Sigma}) &= \boldsymbol{\Sigma} - \boldsymbol{\Sigma}(\boldsymbol{\Sigma} + \sigma_\epsilon^2 \mathbf{I})^{-1}\boldsymbol{\Sigma}, \end{aligned}$$

which can be easily derived from the joint Gaussian distribution of the data \mathbf{Y}_i and the distribution of latent process \mathbf{Z}_i .

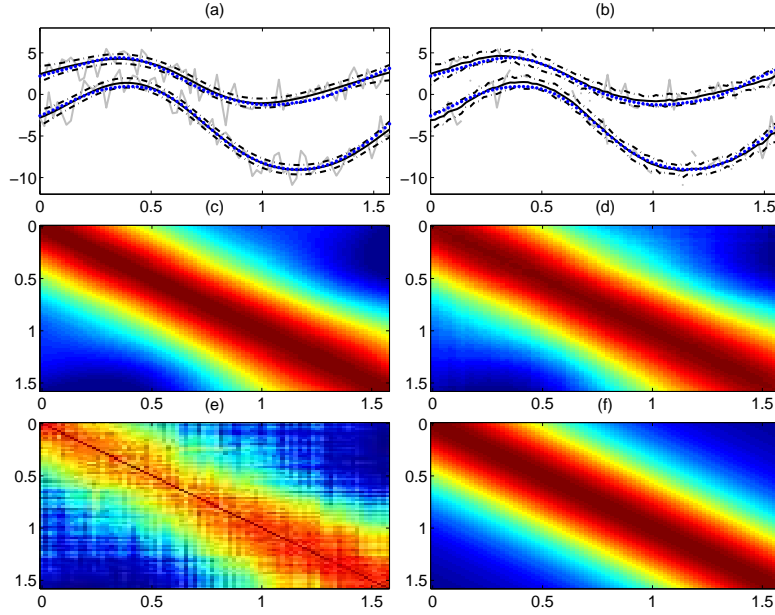


Figure 2: Plots of Simulation 1. (a) 2 example curves for the common grid data (grey lines) superimposed by the Bayesian smoothed estimates (black solid lines) along with the 95% point wise confidence interval (black dashed lines) and the true signals (blue dots); (b) similar curve plots for the uncommon grid case; (c) heat map of the the correlation posterior mean for the common grid case; (d) similar correlation heat map for the uncommon grid case; (e) heat map of the sample correlation estimates (common grid case); (f) the true underlying (Martérn) correlation heat map.

We obtained the the Spline and the Kernel estimates using the R (R Core Team 2013) functions `smooth.spline` and `locpoly` (in the `KernSmooth` package). The smoothing parameter in the former function is determined using generalized cross-validation (GCV) and the bandwidth in the latter function is selected by a direct plug-in approach using the `dpill` function in the `KernSmooth` package. We have chosen `degree = 1` in the `locpoly` function, which corresponds to local linear smoothing. For the Spline and Kernel methods, we also estimate the mean curve by averaging the individually smoothed curves.

To quantitatively measure the goodness of smoothing and estimation, we repeat the above simulation 100 times for the common grid case only, and calculate the root integrated mean square errors (RIMSE), which is defined by $(\int_0^{\pi/2} (\hat{Z}(t) - Z(t))^2 dt)^{1/2}$ where the integration is approximated using trapezoidal rule over the common grid. We report the mean RIMSE by averaging across the 100 simulations and calculate the corresponding standard errors. The results for both smoothed curves and the mean curve estimates are compared with that obtained from the alternative methods in the “Stationary” sections in Table 1.

Table 1: Results in Simulation. The averaged RIMSEs and the corresponding standard errors (in parentheses) for the smoothed curves $Z_i(\mathbf{t})$ and the mean curve $\mu(\mathbf{t})$ using the proposed methods (Bayesian), PACE, cubic splines (Spline) and kernel smoothing (Kernel).

RIMSE	Data	Splines	Kernel	PACE	Bayesian	BLS
$Z_i(\mathbf{t})$	Stationary	0.4234	0.4582	0.4049	0.3723	0.3628
		(0.0019)	(0.0015)	(0.0020)	(0.0017)	(0.0014)
	Non-stationary	0.5209	0.5462	0.4595	0.4453	0.4127
		(0.0020)	(0.0016)	(0.0020)	(0.0015)	(0.0015)
$\mu(\mathbf{t})$	Stationary	0.3917	0.4014	0.3984	0.3846	0.3748
		(0.0154)	(0.0160)	(0.0160)	(0.0157)	(0.0157)
	Non-stationary	0.5318	0.5435	0.5514	0.5183	0.5066
		(0.0211)	(0.0210)	(0.0213)	(0.0208)	(0.0215)

Tables 1 demonstrates that the BLS method provides the smallest RIMSEs and standard errors. This is what we expected since as an “oracle” method, BLS should give the best possible estimator for both $Z_i(\mathbf{t})$ and $\mu(\mathbf{t})$, thus the resulting RIMSEs and the standard errors can be treated as lower bounds for that obtained from all other methods. From the stationary data cases, we see that the proposed Bayesian approach achieves clear improvement on smoothing than the Splines/Kernel/PACE methods (0.3723 vs. 0.4234/0.4582/0.4049 on RIMSE). The mean curve estimates of the Bayesian method is slightly better than the Spline/PACE methods (0.3846 vs. 0.3917/0.3984) and is much better than the Kernel method (0.3846 vs. 0.4014).

In addition to the results in Tables 1, we also calculated the RIMSE for the covariance surface, defined by $(\int_0^{\pi/2} \int_0^{\pi/2} (\hat{\Sigma}(s, t) - \Sigma(s, t))^2 ds dt)^{1/2}$. We compare the RIMSE from the Bayesian method with that from PACE and the sample estimate (Sample), as well as that obtained from the sample estimate using the Bayesian-smoothed curves (Sample Smoothed). The results are listed in the “Stationary” section of Table 2. From Table 2 we observe that the Sample Smoothed method gives the lowest RIMSE, which is slightly smaller than the PACE estimate (1.2450 vs. 1.2583). In this simulation study with stationary Gaussian data, the estimate obtained directly from the Bayesian method has RIMSE lower than the Sample method with raw data and PACE estimate (1.2497 vs. 1.5345 and 1.2583). This is not a surprise to us because from the covariance estimation perspective, the Bayesian method proposed is essentially a Bayesian counterpart of the PACE method. Therefore the covariance estimate obtained should be comparable with

the PACE method.

Table 2: Results in Simulation. The averaged RIMSEs and the corresponding standard errors (in parentheses) for the covariance surface $\Sigma(\mathbf{t}, \mathbf{t})$ using the sample estimate with raw data (Sample), the PACE method, the proposed method (Bayesian) and the sample estimates based on the Bayesian-smoothed curves (Sample Smooth).

RIMSE	Data	Sample	PACE	Bayesian	Sample Smoothed
$\Sigma(\mathbf{t}, \mathbf{t})$	Stationary	1.5345 (0.0378)	1.2583 (0.0420)	1.2497 (0.0440)	1.2450 (0.0433)
	Non-stationary	2.5904 (0.0757)	2.3118 (0.0778)	2.3289 (0.0849)	2.3153 (0.0795)

Table 3: Coverage probability for the 95% point wise credible intervals of $Z_i(\mathbf{t})$, $\mu(\mathbf{t})$, and $\Sigma(\mathbf{t}, \mathbf{t})$.

Data	$Z_i(\mathbf{t})$	$\mu(\mathbf{t})$	$\Sigma(\mathbf{t}, \mathbf{t})$
Stationary (common-grid)	0.9433	0.7250	0.9211
Stationary (sparse)	0.9358	0.8500	1.0000
Non-stationary (common-grid)	0.9632	0.7250	0.9134
Non-stationary (sparse)	0.9420	0.7000	0.8875

In PACE method, covariance is estimated based on pre-smoothed functional data using local linear smoothing. Therefore, the PACE result is more comparable with the Sample estimation with our smoothed data. However, one advantage of using a Bayesian method is that, it is more convenient for us to perform posterior inference for almost all parameters. For example, we can easily construct 95% credible interval for the covariance, whereas in PACE it is not clear how to do accuracy assessment directly from the method, or it might cost even more than our MCMC algorithm to obtain confidence intervals by bootstrapping. We also display the coverage probabilities in Table 3 for the Bayesian 95% credible intervals of $Z_i(\mathbf{t})$, $\mu(\mathbf{t})$, and $\Sigma(\mathbf{t}, \mathbf{t})$. We can see that the coverage probabilities for $Z_i(\mathbf{t})$ and $\Sigma(\mathbf{t}, \mathbf{t})$ are all above 90% for the simulation study with stationary covariance. The low coverage for $\mu(\mathbf{t})$ is due to a narrow band of its 95% credible interval, but the Bayesian estimate of $\mu(\mathbf{t})$ is very close to the truth with the lowest RIMSE as shown in Table 2.

4.2 Simulation 2: functional data with non-stationary covariance

We generate functional data with non-stationary covariance through imposing a nonlinear transformation on the true underlying Gaussian processes generated in Section 4.1. Let $\tilde{X}_i(t)$ denote a Gaussian process generated from Section 4.1 using the Matérn covariance. A non-stationary Gaussian process can be obtained through the transformation $X_i(t) = h(t)\tilde{X}_i(\xi(t))$ where $h(t) = t + 1/2$ and $\xi(t) = (t)^{2/3}$. In

particular, $X_i(t)$ is a Gaussian process with mean $\mu(t) = 3h(t) \sin(4\xi(t))$ and covariance $\Sigma(s, t) = 5h(s)h(t)\text{Matern}_{cor}(|\xi(s) - \xi(t)|; \rho = 1/2, \nu = 3.5)$. Similarly as Simulation 1, in each simulation $n = 100$ non-stationary functional trajectories were generated on the same common grid as in Simulation 1. Furthermore, noise was added to the true smoothed curves similarly as in Simulation 1. Functional data of sparse case (with uncommon grid) were produced in the same way as in Simulation 1.

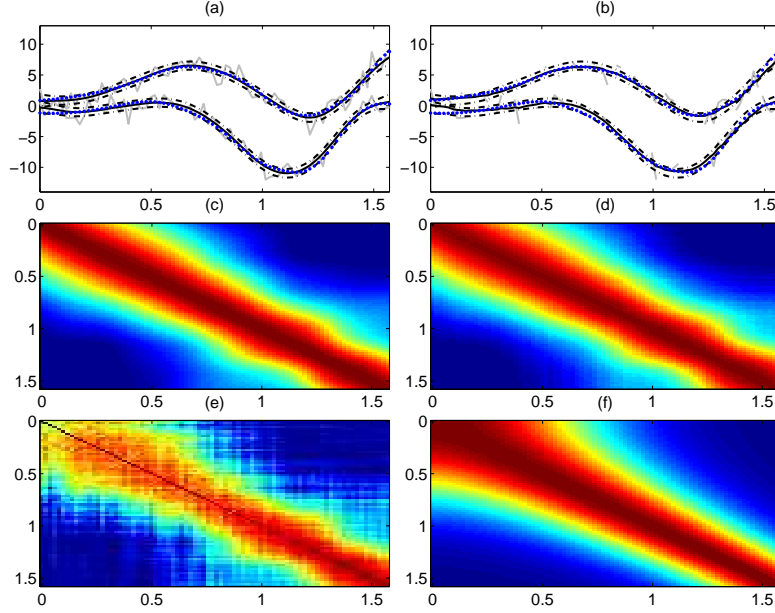


Figure 3: Plots of Simulation 2. (a) 2 example curves for the common grid data (grey lines) superimposed by the Bayesian smoothed estimates (black solid lines) along with the 95% point wise confidence interval (black dashed lines) and the true signals (blue dots); (b) similar curve plots for the uncommon grid case; (c) heat map of the the correlation posterior mean for the common grid case; (d) similar correlation heat map for the uncommon grid case; (e) heat map of the sample correlation estimates (common grid case); (f) the true underlying (non-stationary) correlation heat map.

Two example curves for the common grid and uncommon grid cases were plotted in Figure 3 (a) and (b) respectively. We follow the same way of determining the hyper-parameters and calculating the RIMSE posterior mean for the mean curve and covariance surface. The results are plotted in Figure 3 (a)-(d). We also presented the heat maps of the sample correlation estimate in the common grid case and the true underlying correlation in (e) and (f), respectively. The averaged RIMSEs (across 100 repetitions) for the smoothed curves $Z_i(t)$, the mean curve $\mu(t)$ and the covariance surface $\Sigma(s, t)$ were displayed in the “Non-stationary” section of Table 1 and Table 2. In addition, the coverage probabilities of the 95% Bayesian credible interval for $Z_i(t)$,

$\mu(\mathbf{t})$, and $\Sigma(\mathbf{t}, \mathbf{t})$ were displayed in the “Non-stationary” section of Table 3.

These plots and tables show similar patterns as in the stationary case. In particular, the proposed Bayesian approach gives the best signal and mean signal estimates with the lowest RIMSE. The covariance estimates also follow similar pattern as in the stationary data case. However, from the heat map of the Bayesian correlation estimate (common-grid case) in Figure 3 (c), we can see that the assumed *IWP* prior with stationary scale kernel $\Psi(\cdot, \cdot)$ shrank the Bayesian estimate toward a stationary form. The Bayesian correlation estimates follow the structure of the sample correlation estimate as shown in Figure 3 (c) & (d), but are obviously smoother than the sample estimate. Notice that we have assumed a stationary Matérn structure in the Ψ parameter of the *IWP* prior, which constrains the prior support of *IWP* to be the Matérn family. For non-stationary data, it may be more desirable to choose Ψ using a more flexible structure. For example, we could let $\Psi(\cdot, \cdot) = \sigma_s^2 A(\cdot, \cdot)$, set $A(\cdot, \cdot)$ to be the correlation surface estimated from the data, and set σ_s^2 to be a function of t . One need to be very careful about choosing a proper correlation kernel for $A(\cdot, \cdot)$, such that it is positive definite and symmetric.

5 Case studies with real data

5.1 Spectroscopy data with low volume of noise

In this study, we will analyze a real data set of spectroscopy measurements, which were produced in a cervical pre-cancer diagnosis study and used to help diagnosing cervical cancer in the early stages. The data contains $n = 462$ spectroscopy measurements captured using a multispectral digital colposcope (MDC) device (Buys et al. 2012). When measuring the data, a provider put a probe in contact with patient’s cervix; the device will then eject a beam of light through the probe on patient’s cervix tissue and record the spectrum intensities of the reflected light through a white light filter set. Each measurement contains intensity values (\log_{10} transformed) ranging from 410 to 700 nanometer (nm) in emission wavelengths. Since the spectroscopy data are very dense on the emission wavelengths (common grid), we took intensity values at 1/3 equally spaced emission wavelengths as our observations. We will treat the values at the rest 2/3 wavelengths as validation data to test the prediction performance. Figure 1(a) shows three example curves on their original scale before the \log_{10} transformation.

We applied the proposed Bayesian smoothing method on this real spectroscopy data (\log_{10} transformed, common grid with $n > p$) with $\delta = 5$ and hyper-priors decided by the heuristic empirical Bayesian method in Section 2.2. The values of the prior parameters are: $a_\epsilon = 1117.759$, $b_\epsilon = 1$, $a_s = 0.905$, $b_s = 5$, $\hat{\rho} = 369.7157$, $\nu = 3.19$. The Bayesian estimates for σ_ϵ^2 and σ_s^2 are 9.339×10^{-5} with 95% credible interval $(9.199 \times 10^{-5}, 9.488 \times 10^{-5})$, and 196.655 with 95% confidence interval $(173.679, 220.693)$, respectively.

Example Bayesian smoothed curves are plotted in Figure 1(d), along with individually smoothed curves by Kernel smoothing method in Figure 1(b) and Splines

smoothing method in Figure 1(c). As we can observe from Figure 1, all local wiggles in the raw data were completely wiped out by the Kernel smoothing method, but were kept consistently by the Bayesian smoothing method. Even though the Splines smoothing method also preserved local features, but not in a consistent way for all data curves. This real data study demonstrated that our Bayesian method can borrow strength across all data, thus it is capable of preserving features that were repeated among the data such that little information might be lost after smoothing.

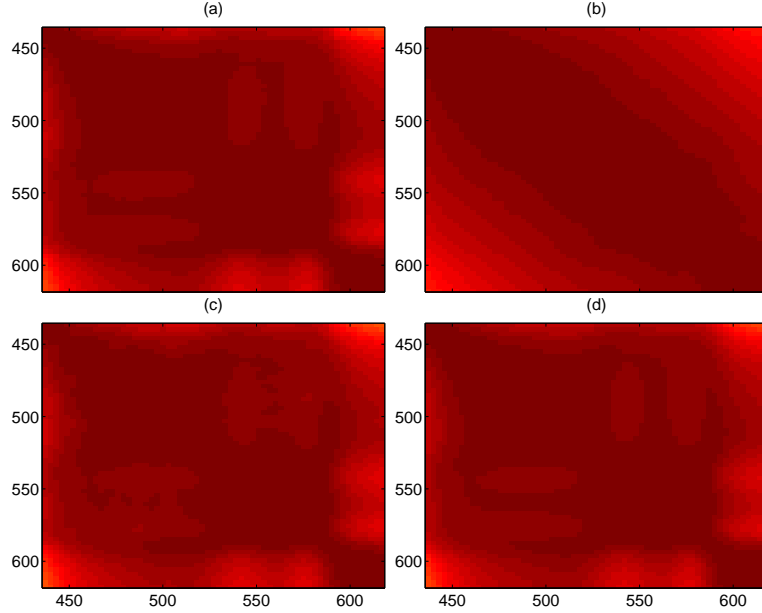


Figure 4: Heat maps of correlation estimates from sample estimation with raw data in (a), BHM in (b), PACE in (c), and sample estimation with Bayesian smoothed data in (d).

Because this real data set contains less amount of noise, we treat the raw data as if it were the true signals. We would expect a good correlation estimate has the same structure as the sample estimate with raw data. From the heat maps of the correlation estimates (Figure 4), we can see that although the Bayesian correlation estimate in Figure 4(b) is mostly like a Matérn because of the Matérn structure we put in the prior, the sample correlation estimate with Bayesian smoothed data in Figure 4(d) is very good. Both sample estimates have very similar structures around emission wavelengths (500, 550) (two slightly low correlated oval regions). The PACE estimate in Figure 4(c) is also very good, but it tends to over smooth the boundary between those two oval regions.

We use data on the remaining 2/3 of the wavelengths as a validation data set to compare the prediction performance of our Bayesian method with that of three

alternative methods – Spline, Kernel and PACE. With Splines smoothing method, the values on the validation grid points can be easily predicted from the estimated basis function coefficients which were obtained by smoothing the “observed” values. For the Kernel/PACE/Bayesian methods, prediction values at the validation points in each curve are obtained using linear interpolation. Due to the low noise level of this spectroscopy data, we simply treat the observed values at the validation wavelengths as the truth and calculate the root mean square errors (RMSE) for all methods. The results are listed in Table 4, which shows that the Bayesian method achieves the smallest RMSE and then demonstrates the benefits of simultaneous smoothing.

Table 4: RMSEs for predictions on validation data.

Splines	Kernel	PACE	Bayesian
0.020	0.039	0.025	0.017

5.2 Metabolic data with high volume of noise

In this real case study, we applied our Bayesian smoothing method on a metabolic data set (collected by the Children’s Nutrition Research Center (CNRC) at Baylor College of Medicine), which consisted with energy expenditure (EE) measurements for 106 children (44 objects with obese and 62 objects without obese). For each child, EE measurements were collected per minute during 24 hours, which can be treated as evaluations of an energy function over time. One wish to compare the data pattern for those two groups of children, with obese or without obese. From the the plot of example EE measurements in Figure 5a (grey curves), we can see that the data obviously have high volume of noise, thus requiring smoothing.

It is intuitive to assume the subdata sets of children with or without obese have different mean and covariance. Therefore, we would apply the Bayesian smoothing method on the subdata sets of children with or without obese, respectively. Here, we only use part of the data (EE measurements of 100 minutes during the sleep time of the obese group) as an example case (common grid with $n < p$) to show the results from our Bayesian smoothing method. In this real case study, we took $\delta = 5$, which lead to rough signal estimates with lots of small wiggles as in Figure 5a (black curves). However, one can easily increase the value of δ to gain more smoothness in the signal estimates. Similarly, we can see that our Bayesian signal estimates are more consistent than the ones from splines smoothing method (Figure 5b), while kept more local features than the kernel smoothing method (Figure 5c).

6 Discussion

We have proposed a unified Bayesian hierarchical model to smooth functional data through borrowing strength across all observations simultaneously, and to estimate the mean curve and covariance surface. The proposed approach applies to functional

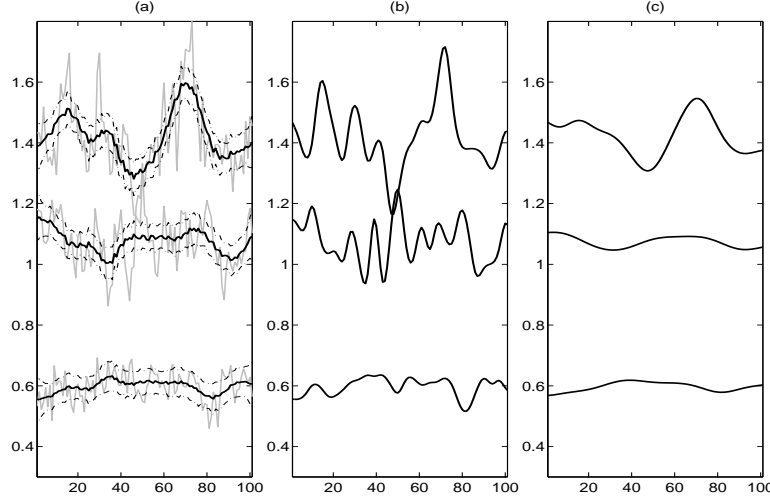


Figure 5: (a): Bayesian signal estimates (black curves) with 95% credible interval (black dashed curves) and raw observations (grey curves); (b): corresponding signal estimates from spline smoothing method; (c): corresponding signal estimates from kernel smoothing method.

data on both common and uncommon grids and can accommodate data with both stationary and non-stationary covariances. Comparing with methods that rely on nonparametric smoothing to each individual curve, this unified Bayesian framework can preserve systematic patterns that are common across all functional observations. The performance on mean and covariance estimation is comparable with that of the frequentist methods such as PACE. Simulation studies have shown that with Bayesian smoothed data, further inference could produce better results than inference based on non-smoothed data. For instance, the sample covariance estimate using Bayesian smoothed data has the lowest RIMSE than all other methods we compared in the simulation studies.

All inference in our Bayesian approach is based on discretizing the Gaussian processes on a grid, to get functional estimates on an arbitrary grid, we can easily interpolate our posterior estimates. One needs to be careful to guarantee symmetry and positive definiteness when interpolating the covariance matrix. Further analysis might require that the smoothed functional observations to be i.i.d.. We would like to note that the smoothed curves obtained from our Bayesian inference will no longer be i.i.d. due to the borrowing of strength across curves, but they will still be exchangeable.

When dealing with functional data on uncommon grids, our approach involves evaluating mean and covariance on the pooled grid, which can be extremely dense and could cause severe numerical problems. For example, the calculation in (10) and (11) involves taking inverse of the covariance matrix $\Sigma(\mathbf{t}_i, \mathbf{t}_i)$. Even when each \mathbf{t}_i is

very sparse, the length of \mathbf{t}_i^* could be as large as thousands. This is a typical problem faced in the Gaussian process regression literature. Many solutions have been proposed to deal with intensive computation and numerical issues caused by dense grid. The essential idea is to approximate the large matrix or its inverse using a low rank matrix. Comprehensive reviews can be found in Rasmussen and Williams (2005, Chapter 8.) and Quiñonero Candela et al. (2007). Banerjee et al. (2012) adopt a linear random projection method for efficient approximation. These techniques can all be integrated into our MCMC steps to further improve the scalability of our method.

We would like to mark that the mean and covariance estimation is by no means a new topic in Bayesian analysis and functional data analysis. Rosen and Thompson (2009) proposed a Bayesian regression model to estimate the mean and covariance for multivariate functional data. Rice and Silverman (1991) developed a method of estimating the mean function non-parametrically under the assumption that it is smooth. They suggested using cross-validation to choose the smoothing parameter, and estimating the covariance structure under the assumption that the first few eigenfunctions are smooth and the eigenvalues decay rapidly. The PACE method of Yao et al. (2005) relies on 2D local linear smoothing to estimate the covariance surface.

Our contribution in this paper is to provide a unified Bayesian framework for smoothing all curves simultaneously and estimating the mean and covariance. One novelty of this method is that imposing a smooth covariance kernel in the hierarchical scale parameter of the IWP prior gives us the flexibility to adjust the smoothness of the signal estimate and the accuracy of the covariance estimate. From the estimation perspective, we consider our method as a Bayesian counterpart of the PACE method. We do not expect our estimation result to always outperform that of PACE. However, Bayesian inference brings us tremendous convenience on inference and accuracy assesment. For example, it provides 95% credible intervals on the smoothed curves, the mean curve, the covariance surface, as well as all other parameters involved, while these uncertainties could be hard to quantify under a frequentist setup.

As shown in the simulation with non-stationary Gaussian data, using a stationary prior for the covariance still produced good smoothing signal estimates, but the Bayesian covariance estimate was shrank toward a stationary structure. In our continuing research, we will investigate how to provide a proper non-stationary smooth covariance kernel for the scale parameter in the IWP prior.

Acknowledgments

The authors very much appreciate for all of the helpful comments from the editor, associate editor, and two referees, which greatly improved the quality of this paper. We want to thank all colleagues in the PO1 project (supported by NIH grant PO1-CA-082710) for collecting the spectroscopy data and the Children’s Nutrition Research Center at Baylor College of Medicine (supported by grant ...) for providing the metabolic data.

References

- Banerjee, A., Dunson, D. B., and Tokdar, S. T. (2012). “Efficient Gaussian process regression for large datasets.” *Biometrika*, 1–15.
- Buys, T. P., Cantor, S. B., Guillaud, M., Adler-Storthz, K., Cox, D. D., Okolo, C., Arulogon, O., Oladepo, O., Basen-Engquist, K., Shinn, E., et al. (2012). “Optical technologies and molecular imaging for cervical neoplasia: a program project update.” *Gender medicine*, 9(1): S7–S24.
- Cardot, H., Ferraty, F., and Sarda, P. (2003). *Statistica Sinica*, 13(3): 571–592.
- Dawid, A. P. (1981). “Some matrix-variate distribution theory: notational considerations and a Bayesian application.” *Biometrika*, 68(1): 265–274.
- Gelman, A. and Rubin, D. B. (1992). “Inference from iterative simulation using multiple sequences.” *Statistical science*, 457–472.
- Hall, P., Poskitt, D. S., and Presnell, B. (2001). “A Functional DataAnalytic Approach to Signal Discrimination.” *Technometrics*, 43(1): 1–9.
- Hitchcock, D. B., Casella, G., and Booth, J. G. (2006). “Improved estimation of dissimilarities by presmoothing functional data.” *Journal of the American Statistical Association*, 101(473): 211–222.
- Quiñonero Candela, J., E., R. C., and Williams, C. K. I. (2007). “Approximation Methods for Gaussian Process Regression.” Technical report, Applied Games, Microsoft Research Ltd.
- R Core Team (2013). *R: A Language and Environment for Statistical Computing*. R Foundation for Statistical Computing, Vienna, Austria.
URL <http://www.R-project.org/>
- Ramsay, J. O. (2006). *Functional data analysis*. Wiley Online Library.
- Ramsay, J. O. and Dalzell, C. (1991). “Some tools for functional data analysis.” *Journal of the Royal Statistical Society. Series B (Methodological)*, 539–572.
- Ramsay, J. O. and Silverman, B. W. (2002). *Applied functional data analysis: methods and case studies*, volume 77. Springer New York.
- Rasmussen, C. E. and Williams, C. K. I. (2005). *Gaussian Processes for Machine Learning (Adaptive Computation and Machine Learning)*. The MIT Press.
- Rice, J. A. and Silverman, B. W. (1991). “Estimating the Mean and Covariance Structure Nonparametrically When the Data Are Curves.” *Journal of the Royal Statistical Society, Series B*, 53: 233–243.
- Rosen, O. and Thompson, W. K. (2009). “A Bayesian regression model for multivariate functional data.” *Computational Statistics & Data Analysis*, 53(11): 3773–3786.

- Särkkä, S. and Aki, V. (2014). “MCMC Diagnostics for Matlab.” <http://becs.aalto.fi/en/research/bayes/mcmcdiag/>.
- Stein, M. L. (1999). *Interpolation of spatial data: some theory for kriging*. Springer.
- Von Neumann, J. (1941). “Distribution of the ratio of the mean square successive difference to the variance.” *The Annals of Mathematical Statistics*, 12(4): 367–395.
- Yao, F., Müller, H.-G., and Wang, J.-L. (2005). “Functional linear regression analysis for longitudinal data.” *The Annals of Statistics*, 33(6): 2873–2903.
- Zhang, H. (2004). “Inconsistent estimation and asymptotically equal interpolations in model-based geostatistics.” *Journal of the American Statistical Association*, 99(465): 250–261.
- Zhu, H. and Cox, D. D. (2009). *A Functional Generalized Linear Model with Curve Selection in Cervical Pre-Cancer Diagnosis using Fluorescence Spectroscopy*, volume 57. Beachwood, Ohio, USA: Institute of Mathematical Statistics.
- Zhu, H., Strawn, N., and Dunson, D. B. (2011). “Bayesian graphical models for multivariate functional data.” *Technical Report*.
- Zhu, H., Vannucci, M., and Cox, D. D. (2010). “A Bayesian Hierarchical Model for Classification with Selection of Functional Predictors.” *Biometrics*, 66: 463–473.